



Comprehensive Expression Analysis of Cardiac Fibroblast Growth Factor 23 in Health and Pressure-induced Cardiac Hypertrophy

Fiona Eitner^{1†}, Beatrice Richter^{1†}, Saskia Schwänen¹, Malgorzata Szaroszyk², Isabel Vogt¹, Andrea Grund¹, Thomas Thum³, Joerg Heineke^{2,4}, Dieter Haffner¹ and Maren Leifheit-Nestler^{1*}

OPEN ACCESS

Edited by:

Trayambak Basak,
Indian Institute of Technology Mandi,
India

Reviewed by:

Miriam Zacchia,
University of Campania Luigi Vanvitelli,
Italy
Ronald J. Vagnozzi,
University of Colorado Anschutz
Medical Campus, United States

*Correspondence:

Maren Leifheit-Nestler
leifheit-nestler.maren@mh-
hannover.de

†These authors have contributed
equally to this work

Specialty section:

This article was submitted to
Molecular and Cellular Pathology,
a section of the journal
Frontiers in Cell and Developmental
Biology

Received: 08 October 2021

Accepted: 13 December 2021

Published: 18 January 2022

Citation:

Eitner F, Richter B, Schwänen S,
Szaroszyk M, Vogt I, Grund A, Thum T,
Heineke J, Haffner D and
Leifheit-Nestler M (2022)
Comprehensive Expression Analysis of
Cardiac Fibroblast Growth Factor 23 in
Health and Pressure-induced
Cardiac Hypertrophy.
Front. Cell Dev. Biol. 9:791479.
doi: 10.3389/fcell.2021.791479

¹Department of Pediatric Kidney, Liver and Metabolic Diseases, Pediatric Research Center, Hannover Medical School, Hannover, Germany, ²Department for Cardiology and Angiology, Hannover Medical School, Hannover, Germany, ³Institute of Molecular and Translational Therapeutic Strategies, Hannover Medical School, Hannover, Germany, ⁴Department of Cardiovascular Physiology, European Center for Angioscience (ECAS), Medical Faculty Mannheim, University of Heidelberg, Mannheim, Germany

Enhanced fibroblast growth factor 23 (FGF23) is associated with left ventricular hypertrophy (LVH) in patients with chronic kidney and heart disease. Experimentally, FGF23 directly induces cardiac hypertrophy and vice versa cardiac hypertrophy stimulates FGF23. Besides the bone, FGF23 is expressed by cardiac myocytes, whereas its synthesis in other cardiac cell types and its paracrine role in the heart in health and disease is unknown. By co-immunofluorescence staining of heart tissue of wild-type mice, we show that Fgf23 is expressed by cardiac myocytes, fibroblasts and endothelial cells. Cardiac Fgf23 mRNA and protein level increases from neonatal to six months of age, whereas no age-related changes in bone *Fgf23* mRNA expression were noted. Cardiac myocyte-specific disruption of *Fgf23* using Cre-LoxP system (*Fgf23^{fl/fl}/cre⁺*) caused enhanced mortality, but no differences in cardiac function or structure. Although pressure overload-induced cardiac hypertrophy induced by transverse aortic constriction (TAC) resulted in a slightly worse phenotype with a more severe reduced ejection fraction, higher end-systolic volume and more enlarged systolic LV diameter in *Fgf23^{fl/fl}/cre⁺* mice compared to controls, this was not translated to any worse cellular hypertrophy, fibrosis or chamber remodeling. TAC induced *Fgf23* mRNA expression in whole cardiac tissue in both genotypes. Interestingly, co-immunofluorescence staining revealed enhanced Fgf23 synthesis in cardiac fibroblasts and endothelial cells but not in cardiac myocytes. RNA sequencing of isolated adult cardiac myocytes, cardiac fibroblasts and endothelial cells confirmed significantly higher *Fgf23* transcription in cardiac fibroblasts and endothelial cells after TAC. Our data indicate that Fgf23 is physiologically expressed in various cardiac cell types and that cardiac fibroblasts and endothelial cells might be an important source of FGF23 in pathological conditions. In addition, investigations in *Fgf23^{fl/fl}/cre⁺* mice suggest that cardiac myocyte-derived FGF23 is needed to maintain cardiac function during pressure overload.

Keywords: FGF23, cardiac myocytes, cardiac fibroblasts, endothelial cells, left ventricular hypertrophy, fibrosis, transverse aortic constriction

INTRODUCTION

Chronic kidney disease (CKD) is a worldwide health problem, and CKD patients suffer from an excessive high risk for cardiovascular disease (CVD) (Sarnak et al., 2003; Eckardt et al., 2013). Over 70% of patients with end-stage kidney disease (ESKD) develop pathological cardiac remodeling including hypertrophy and fibrosis, which promotes diastolic dysfunction, arrhythmia, heart failure and sudden death (Van Berlo et al., 2013; Ham et al., 2018). Hereby, the involvement of the bone-derived hormone fibroblast growth factor (FGF) 23 is widely discussed (Riminucci et al., 2003).

FGF23 synthesis in bone is induced in response to various stimuli to maintain phosphate homeostasis (Shimada et al., 2004; Shimada et al., 2005; Kawata et al., 2007; De Borst et al., 2011; Haussler et al., 2012; Rodriguez-Ortiz et al., 2012). Physiologically, FGF23 exerts its renal functions by binding to FGF receptor (FGFR) 1 in proximal tubular cells in the presence of its co-factor klotho causing intracellular activation of mitogen-activated protein kinase (MAPK) signaling leading to increased renal phosphate excretion and decreased 1,25-dihydroxy vitamin D synthesis (Shimada et al., 2004; Urakawa et al., 2006). CKD is a state of high phosphate load and therefore FGF23 levels in the circulation already start to rise in early stages of CKD and reach a 1,000-fold increase in ESKD (Weber et al., 2003; Gutierrez et al., 2005). In parallel, the prevalence of left ventricular hypertrophy (LVH) increases and is associated with a higher mortality rate in these patients (Go et al., 2004; Paoletti et al., 2016). Furthermore, increased circulating FGF23 in CKD is linked to LVH development and mortality (Faul et al., 2011). *In vitro* and *in vivo* data show that FGF23 induces LVH by directly targeting the heart *via* binding and phosphorylating the intracellular receptor kinase domain of FGFR4 leading to the activation of the pro-hypertrophic calcineurin/nuclear factor of activated T cells (NFAT) signaling pathway in a klotho-independent manner (Faul et al., 2011; Grabner et al., 2015). Interestingly, studies in the general population have shown that elevated FGF23 levels are also associated with CVD and mortality independent of the presence of CKD (Kestenbaum et al., 2014; Lutsey et al., 2014). Furthermore, FGF23 promotes myocardial fibrosis *via* activation of β -Catenin (Hao et al., 2016), activates the intra-cardiac renin-angiotensin-aldosterone system (RAAS), which in turn promotes LVH and cardiac fibrosis (Böckmann et al., 2019), and it is associated with endothelial dysfunction in CKD patients (Yilmaz et al., 2010), and in human coronary artery endothelial cells *in vitro* (Richter et al., 2016).

FGF23 expression is not limited to the bone since its synthesis has been also found in the heart in cardiac myocytes (Fon Tacer et al., 2010; Andrukhova et al., 2015; Hao et al., 2016; Leifheit-Nestler et al., 2016; Kuga et al., 2020) and in human coronary arteries in patients with impaired kidney function (Van Venrooij et al., 2014). However, its expression in non-myocytes is still controversially discussed (Schumacher et al., 2019). Likewise, the impact of cardiac-derived FGF23 and its possible paracrine actions in the heart in comparison to endocrine-acting FGF23 secreted from bone in health and disease are largely elusive (Leifheit-Nestler et al., 2018).

Here, we show that Fgf23 is expressed in the left as well as the right ventricle and in the respective atria in healthy wild-type mice. In addition to cardiac myocytes, cardiac fibroblasts and endothelial cells synthesize Fgf23 too. To more finely examine the function of cardiac-derived Fgf23, we generated conditional Fgf23 knockout mice by cross-breeding mice with LoxP-flanked (floxed) *Fgf23* alleles with mice harboring a cardiac myocyte-specific recombination. Cardiac myocyte-specific *Fgf23* knockout mice showed normal cardiac phenotype under basic conditions, but exhibited a slightly worse cardiac function after transverse aortic constriction (TAC) in comparison to TAC-operated controls that however, was not translated to any worse cellular hypertrophy, fibrosis or chamber remodeling. Interestingly, cardiac myocyte-specific *Fgf23* knockout mice showed elevated *Fgf23* expression in total cardiac tissue after TAC, raising the question whether cardiac fibroblasts and endothelial cells might be an important source of FGF23 in pathological conditions.

MATERIALS AND METHODS

Generation of Conditional Cardiac Myocyte-specific *Fgf23* Knockout Mice

Animal experiments were approved by the State Office Committee for Animal Welfare Lower Saxony (LAVES, #15/1912) in accordance with national animal protection guidelines from Directive 2016/63/EU of the European Parliament on the protection of animals used for scientific purposes. Mice were housed with a 12:12 h light-dark cycle, had free access to water and fed *ad libitum* with standard rodent chow. The Myh7-Cre mouse line expressing Cre recombinase linked to a Myh7 promoter (B6;129S1-Tg(Myh7-Cre)1Jmk) was kindly provided by Prof. Joerg Heineke (Department of Cardiovascular Physiology, European Center for Angioscience (ECAS), Medical Faculty Mannheim, University of Heidelberg, Mannheim, Germany) and described elsewhere (Heineke et al., 2007). Fgf23 floxed mice were generated based on CRISPR/Cas9 technology by InGenious Targeting, Inc. (Ronkonkoma, NY, United States). To obtain mice with cardiac myocyte-specific *Fgf23* deletion, homozygous *Fgf23^{fl/fl}* mice (B6-Fgf23^{tm1Mln}) were interbred with B6;129S1-Tg(Myh7-Cre)1^{Jmk}. *Fgf23^{fl/fl}/cre⁻* littermates were used as controls.

For genotyping, earmarks were lysed in proteinase K buffer overnight. After deactivation of proteinase K, multiplex PCR was performed to amplify genomic DNA using primer for *Fgf23* floxed allele (forward: AGA TTC CAT TTA CAG TGC CCC TTG G; reverse: ACT TCA GTT ACC TGA AGT CCC AGT TGG) and Myh7-Cre (forward: GGC GTT TTC TGA GCA TAC CT; reverse: CTA CAC CAG AGA CGG AAA TCC). PCR was run for 3 min at 94°C and 31 cycles of 30 s at 94°C, 45 s at 58°C, and 1 min at 72°C, followed by 10 min at 72°C. Samples were separate on a 3% agarose gel including GelRed Nucleic Acid Gel Stain (Biotrend) at 120 V for 60 min and analyzed with a Gel DocTMXR+ (Bio-Rad Laboratories).

Respective male and female *Fgf23^{fl/fl}/cre⁻* and *Fgf23^{fl/fl}/cre⁺* mice with the age of 0 (neonatal), 1, 3 and 6 months were

analyzed. Femur, tibia, and calvaria were isolated and snap-frozen in liquid nitrogen. Isolated mouse hearts were washed in ice-cold PBS followed by 0.5% potassium chloride and cut into three cross-sections. For histological evaluation, the mid cross-section was fixated in 4% RotiHistofix (Carl Roth) and embedded in paraffin. The other two cross-sections were snap-frozen in liquid nitrogen and stored at -80°C for molecular and biochemical analyses.

Transthoracic Echocardiography and Cardiac Catheterization

Echocardiography was performed using the Vevo 2100 Imaging System (FUJIFILM VisualSonics Inc.) as described previously (Zacchigna et al., 2021). Anesthesia was induced with 3% isoflurane and maintained with 0.5–1% isoflurane over a breathing mask. Heart views were acquired in parasternal long axis in B- and M-mode, and short axis in M-mode. All echocardiographic images were analyzed using the Vevo Lab 3.2.0 software.

Cardiac catheterization was performed with PowerLab 16/35 (Millar Instruments). Anesthesia was initialized with 3% isoflurane and maintained with 0.8% isoflurane. The measurements were performed on the opened thorax using the polyamide catheter PVR 1045 (Millar Instruments) and analyzed with the software LabChart 8 (AD Instruments).

Transverse Aortic Constriction

Transverse aortic constriction (TAC) or sham surgery was performed in eight-week-old male and female $\text{Fgf23}^{\text{fl/fl}}/\text{cre}^{-}$ and $\text{Fgf23}^{\text{fl/fl}}/\text{cre}^{+}$ mice by subjecting the aorta to a defined constriction as previously described (Grund et al., 2019a). In brief, a 7–0 silk suture was tied around the aortic arch between the branches of the brachiocephalic trunk and the left common carotid artery and a blunted 27-gauge needle, after which the needle was removed to create a defined constriction. The procedure for sham-operated animals was identical, but the aorta was not ligated. Two weeks after surgery, mice were sacrificed as described above.

Cardiac specific cell types were isolated from mice after sham and TAC as previously described (Appari et al., 2017). In brief, ventricular cardiac myocytes were isolated using a Langendorff system, cardiac endothelial cells and fibroblasts were isolated using MACS technology with CD146 microbeads followed by feeder removal microbeads (Miltenyi Biotec). All isolated cell types were directly used for RNA extraction according to standard protocol followed by deep-sequencing analysis as previously described (Grund et al., 2019b).

Cardiac Magnetic Resonance Imaging

Cardiac magnetic resonance imaging (MRI) was performed for TAC or sham-operated $\text{Fgf23}^{\text{fl/fl}}/\text{cre}^{-}$ and $\text{Fgf23}^{\text{fl/fl}}/\text{cre}^{+}$ mice. Cardiac MRI images were recorded with a Bruker 7T Pharmascan 70/16 (Bruker). Anesthesia was induced with 3% isoflurane and maintained with 0.5% isoflurane. First, a positioning scan was performed, followed by images in 9–10 stacks. For every stack, images were made to encompass an entire

heart cycle. All cardiac MRI images were analyzed with Mass4Mice 7.1 software (MEDIS Medical Technologies). Epicardium and endocardium were marked manually to ascertain left ventricular (LV) mass, end-systolic (ES) and end-diastolic (ED) volume, stroke volume (SV), cardiac output, and ejection fraction (EF). In addition, LV wall geometry was determined at the level of papillary muscles. With regard to slice thickness, papillary muscles were included in the LV cavity.

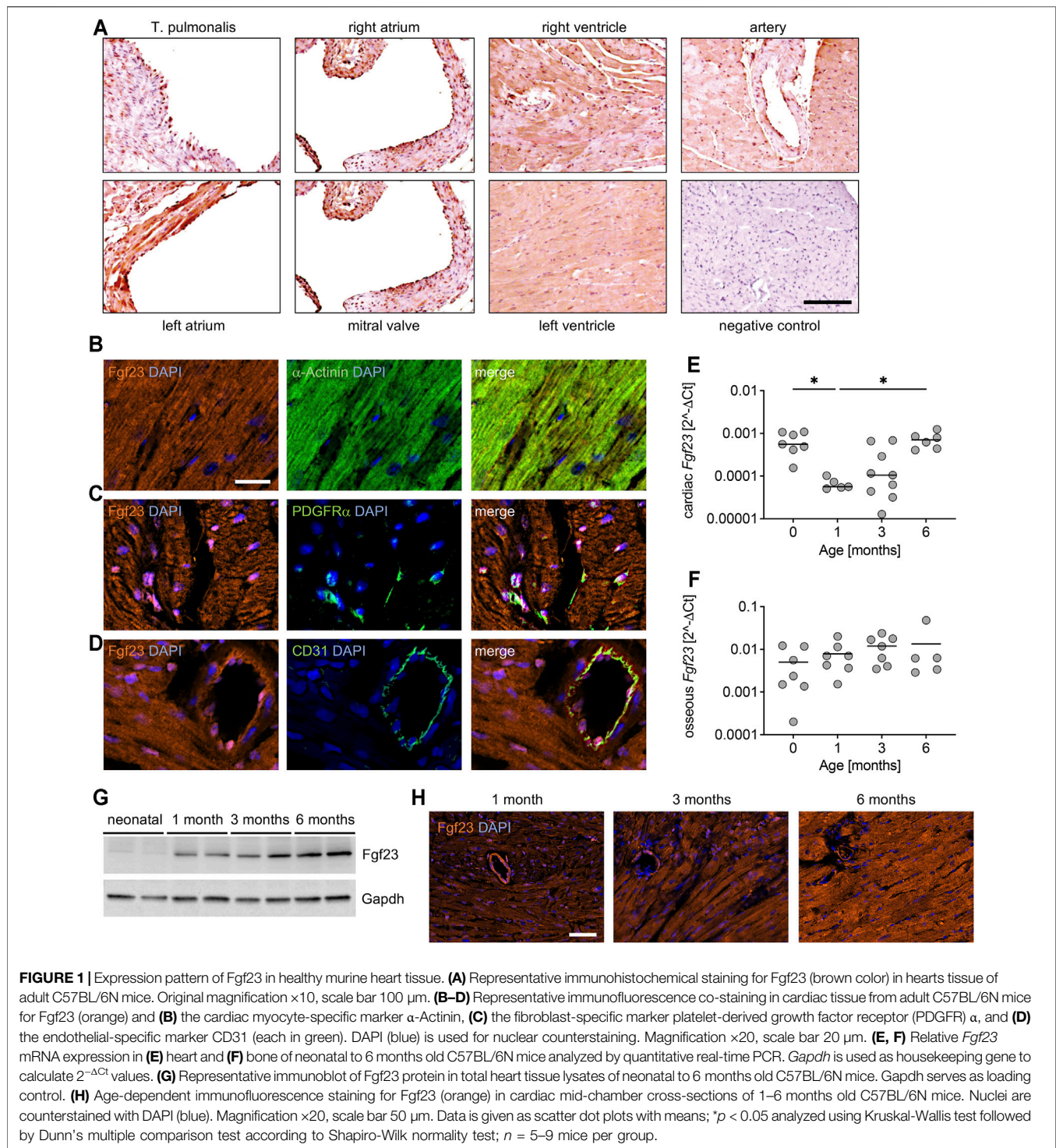
Blood and Urine Biochemistry

Plasma was analyzed for total FGF23 (#60-6300) and intact FGF23 (#60-6800) by ELISA (both from Immotopics). Urine and serum biochemistry were measured on a cobas c111 system (Roche Diagnostics) using Calcium Gen.2, Phosphate ver.2 and creatinine Creatinine Jaffé Gen.2 (all from Roche Diagnostics). No urine was available for one month old $\text{Fgf23}^{\text{fl/fl}}/\text{cre}^{+}$ and $\text{Fgf23}^{\text{fl/fl}}/\text{cre}^{-}$ mice.

Histological Staining of Heart Tissue and Quantification of Cardiac Myocyte Size, Capillarization and LV Fibrosis

Three μm thick cardiac mid-chamber sections were deparaffinized in xylene and hydrated using a descending alcohol series. Hematoxylin and eosin (HE) staining was performed using Meyers hematoxylin and eosin G (Merck Millipore). To visualize interstitial cardiac fibrosis, sections were incubated using picosirius red solution (Merck Millipore) in 1.2% picric acid. For immunohistochemical staining of FGF23 in heart tissue, antigen retrieval was done in citrate buffer pH 6.0, followed by inhibition of endogenous peroxidase activity by hydrogen peroxidase and blocking with 10% normal goat serum in PBS. After incubation with anti-FGF23 primary antibody (Bioss #bs-5768R, dilution 1:200), sections were incubated with horseradish peroxidase-conjugated goat anti-rabbit (Jackson ImmunoResearch #111-035-144, dilution 1:100), followed by incubation with diaminobenzidine substrate (Thermo Scientific #34065) and counterstaining with hematoxylin. Images were taken with either 10x (HE) or 20x objective using the Axio Observer Z1 microscope (Carl Zeiss). To quantify interstitial cardiac fibrosis, five pictures per mouse of the left ventricle were taken using 20x magnification followed by quantification using ImageJ (Böckmann et al., 2019).

For visualization of cell type-specific expression of FGF23, cardiac tissue was stained for anti-CD31 (R&D systems #AF3628; dilution 1:100 in 5% milk in TBST), followed by donkey-anti-goat Alexa Fluor 480 secondary antibody (Invitrogen #A11055, dilution 1:500), anti- α -Actinin (Sigma-Aldrich #A7732, dilution 1:100), followed by goat-anti-mouse Alexa Fluor 660 secondary antibody (Invitrogen #A21054, dilution 1:500), or anti-PDGFR α (R&D Systems #AF1062, dilution 1:100), followed by donkey-anti-goat Alexa Fluor 480 secondary antibody. Afterwards, tissues were stained with anti-FGF23 (Bioss #bs-5768R, dilution 1:200), followed by goat-anti-rabbit Alexa Fluor 555 secondary antibody (Invitrogen #A21428, dilution 1:500). All primary



antibodies were incubated over night at 4°C, and secondary antibodies were incubated for 90 min at room temperature. For measurement of capillarization and cardiac myocyte size, the staining with CD31 was followed by incubation with 5 $\mu\text{g}/\text{ml}$ wheat germ agglutinin (WGA)Alexa Fluor 555 (Invitrogen #W32464) for one hour. Nuclear counterstaining in immunofluorescence was performed with DAPI. All images

were taken with a 20x objective on a Zeiss Axio Observer Z1 microscope (Carl Zeiss) and quantification of cardiac myocyte area was performed with 100 cells per animal using the Zen 2.3 lite software (Carl Zeiss). For quantification of capillarization, five images in 20x magnification per animal were taken and number of capillaries were divided by number of cardiac myocytes per power field.

RNA Isolation, cDNA Synthesis and Quantitative Real-Time PCR Analysis

The RNeasy Mini Kit was used according to manufacturer's protocol for total RNA isolation from murine heart and cardiac specific cell types. For murine bone (either calvaria or femur), the RNeasy Lipid Tissue Kit was used. 500 ng RNA was transcribed into cDNA according to the data sheet of the QuantiTect Reverse Transcription Kit. Real-time polymerase chain reaction (PCR) was performed in triplets using the QuantiFAST SYBR Green PCR Kit (all kits from Qiagen) on a 7900 HT Fast RT-PCR System (Thermo Fisher Scientific) and analyzed using the SDS Software v2.4 (Thermo Fisher Scientific). For murine primer sequences see **Supplementary Table S1**. Relative gene expression levels of *Fgf23*^{fl/fl}/*cre*⁺ mice compared to control were calculated using the $2^{-\Delta\Delta C_t}$ method, with *Gapdh* and *18s* (in bone) serving as housekeeping genes. For *Fgf23* mRNA quantification in **Figures 1, 4**, $2^{-\Delta C_t}$ values were used.

Protein Isolation and Western Blot Analysis

Protein isolation of murine heart tissue was performed with the TissueLyser LT (Qiagen) using RIPA buffer with proteinase and phosphatase inhibitors (Sigma-Aldrich). Samples were incubated at 4°C for 30 min followed by sonification. Protein concentrations were measured *via* BCA assay (Thermo Fisher Scientific) according to manufacturer's protocol.

100 µg total protein was separated on a 12% SDS-gel and transferred on nitrocellulose membrane in transfer buffer containing 18% methanol for 1 h. Membranes were blocked in 5% milk in TBS containing 0.05% Tween-20 for 1 h, afterwards primary antibodies were incubated over-night at 4°C (FGF23-6310 Goat mAb, dilution 1:500, Immotopics; GAPDH 14C10 Rabbit mAb, dilution 1:1,000, Cell Signaling Technology). After washing, secondary antibodies were incubated for 1 h at room temperature (Goat anti-rabbit IgG HRP, dilution 1:1,000, Santa Cruz; Donkey anti-goat IgG HRP, dilution 1:2000, R and D Systems). ECL development was done with the SuperSignal West Femto Maximum Sensitivity Substrate (Thermo Fisher Scientific) and signals were detected with the Odyssey FC Imaging System (LI-COR Bioscience). Expression levels were quantified with the Image Studio Lite 5.2 software (LI-COR Bioscience).

Statistical Analyses

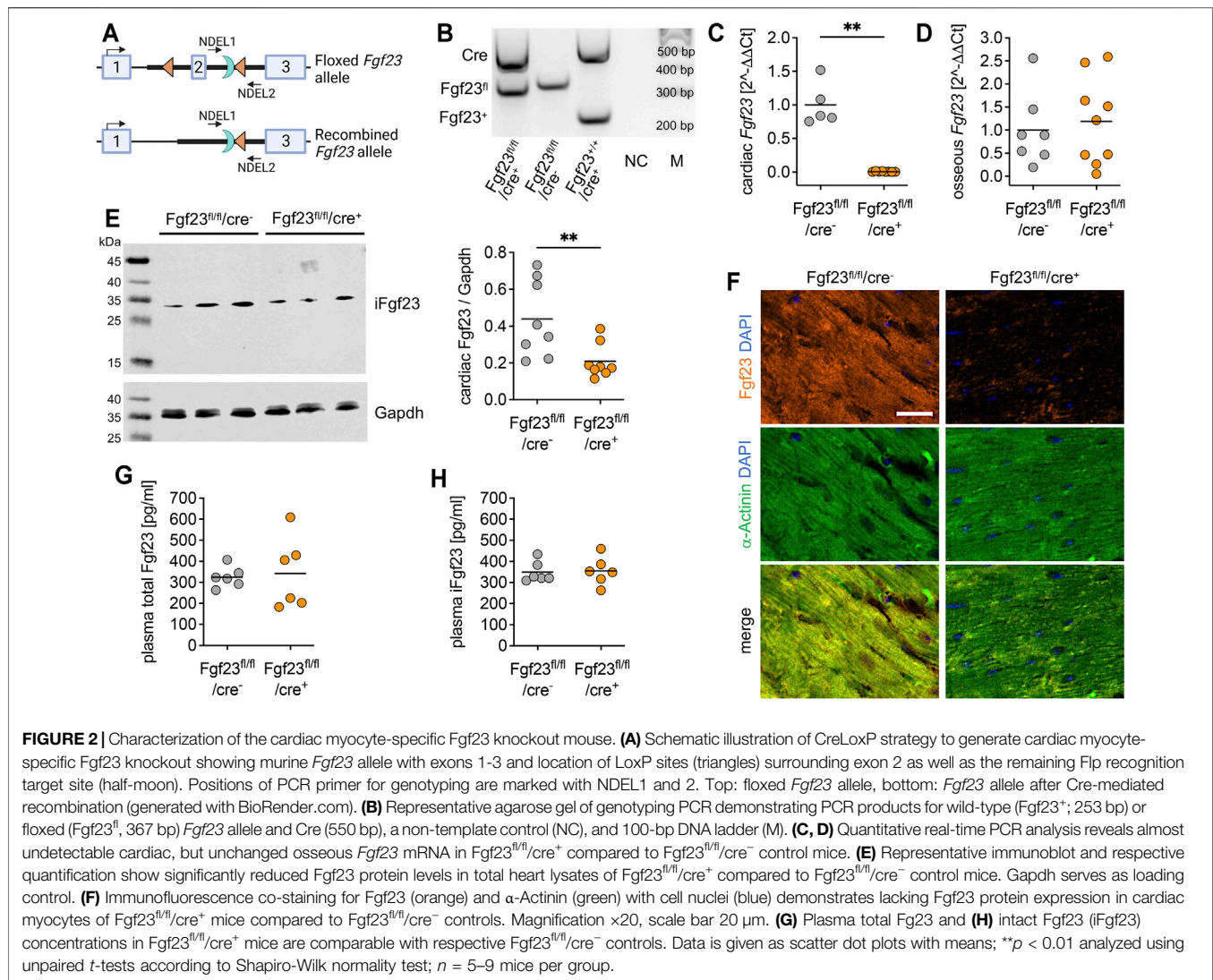
All statistical analyses were performed using GraphPad Prism software 7 (GraphPad Software) Gaussian's distribution was analyzed by Shapiro-Wilk test. Differences between two groups were determined using 2-tailed Students *t*-test or Mann Whitney *U* test, respectively. For time-dependent analyses, one-way ANOVA or Kruskal-Wallis test followed by Dunnett or Dunn's multiple comparison tests were used. TAC-experiments were analyzed by two-way ANOVA followed by Tukey's multiple comparison test. *p* values < 0.05 were considered as statistically significant.

RESULTS

The Healthy Murine Heart Is a Source of Fgf23

Most clinical and experimental studies over the past decade focused on FGF23 in the context of LV pathologies (Faul et al., 2011; Grabner et al., 2015; Matsui et al., 2018). It has not been investigated so far in which areas of the whole heart *Fgf23* is locally expressed. Therefore, we first performed immunohistochemical staining for *Fgf23* using longitudinal sections of healthy adult C57BL/6N wild-type mice. The expression of *Fgf23* was comparable between the left and the right ventricle (**Figure 1A**). In direct comparison, the synthesis of *Fgf23* was higher in the left atrium than in the right atrium (**Figure 1A**). *Fgf23* was clearly expressed in all regions of endocardium and endothelium (**Figure 1A**), while it appeared to be only minimal in the *tunica media* of the depicted vessels, which is predominantly composed of vascular smooth muscle cells (**Figure 1A**). To further elucidate the expression pattern of murine *Fgf23* within specific cardiac cell types, we performed co-immunofluorescence staining of *Fgf23* with cell type specific markers for cardiac myocytes, fibroblasts and endothelial cells in formalin-fixed paraffin-embedded cardiac cross-sections of adult C57BL/6N wild-type mice. *Fgf23* was co-localized with the cardiac myocyte-specific marker α -Actinin, verifying, that healthy cardiac myocytes express *Fgf23* (**Figure 1B**). *Fgf23* was further expressed in platelet-derived growth factor receptor A (PDGFR α) positive cardiac fibroblast (**Figure 1C**) and co-localized with CD31, known as platelet endothelial cell adhesion molecule-1 (PECAM-1), suggesting the expression of *Fgf23* in endothelial cells of the murine heart, too (**Figure 1D**).

Studies in humans showed that circulating total FGF23 is highest in infants and adolescents and lowest at adult age (Fischer et al., 2012), but the age-dependent synthesis of FGF23 in the heart and bone has not been studied so far. Therefore, we next investigated the *Fgf23* expression in heart and bone tissue of C57BL/6N mice from neonatal (0) to 6 months of age. Although the individual variability of mice was high, cardiac *Fgf23* mRNA levels were significantly lower in 1 month old mice compared to neonates and increased again with increasing age (**Figure 1E**), whereas no age-related changes in bone *Fgf23* mRNA expression were noted (**Figure 1F**). Of note, osseous expression of *Fgf23* was approximately 20-fold higher than in the heart. Immunoblot analysis of total cardiac tissue confirmed an age-dependent increase of *Fgf23* protein synthesis (**Figure 1G**), which was verified by immunofluorescence staining of *Fgf23* in cardiac mid-chamber cross-sections (**Figure 1H**). It appears that the increasing total amount of cardiac *Fgf23* originates mainly from cardiac myocytes and that expression in endothelial cells and fibroblasts remains approximately the same with increasing age.

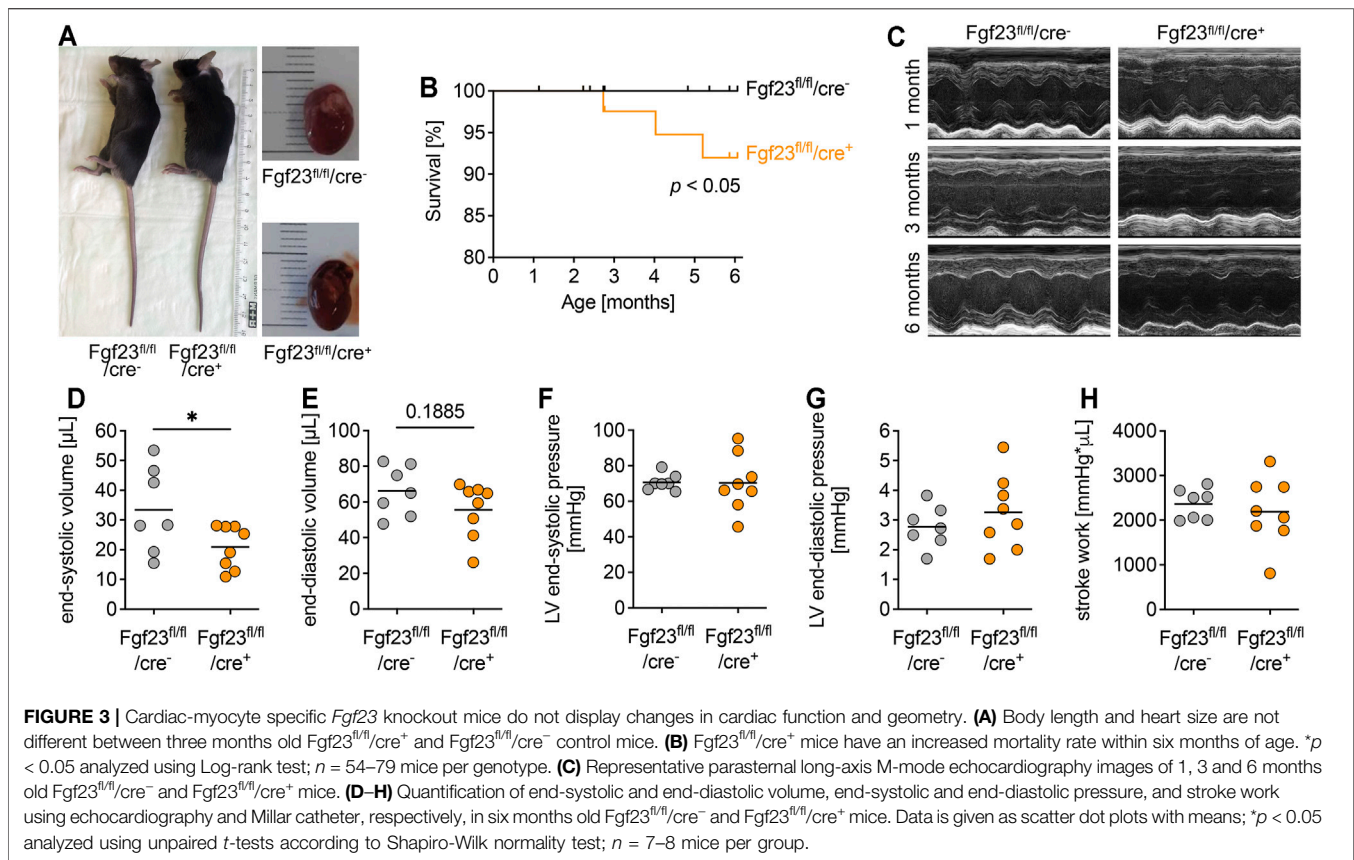


Taken together, *Fgf23* is not only expressed in cardiac myocytes, but also in cardiac fibroblasts and endothelial cells, suggesting that the heart is a source of *Fgf23*.

Mice With Cardiac Myocyte-specific *Fgf23* Deletion Reveal Normal Circulating *Fgf23* Levels

The physiological role of bone-derived endocrine-acting FGF23 in renal phosphate homeostasis is well-established (Shimada et al., 2004), whereas the role of intra-cardiac FGF23 synthesis has been poorly studied. To investigate cardiac-derived FGF23 in more detail, we generated a cardiac myocyte-specific *Fgf23* knockout mouse using Cre-LoxP system (Figure 2A). The first LoxP site was inserted 222 bp upstream of exon 2 and the Neo cassette, containing the second LoxP site, was inserted 342 bp downstream of exon 2. The size of the target region was 668 bp containing exon 2. The respective *Fgf23*-LoxP construct was delivered to iTL BF1 (C57BL/6 FLP) embryonic stem cells,

which were microinjected into Balb/c blastocysts using standard protocols. Resulting chimeras with high percentage black fur color were mated to C57BL/6 wild-type mice to generate germline floxed *Fgf23* mice. After intercrossing *Fgf23*^{fl/+} mice, homozygous non-recombined *Fgf23*-LoxP mice (*Fgf23*^{fl/fl}) were mated with transgenic cardiac myocyte-specific B6;129S1-Tg(Myh7-Cre)^{1Jmk} mice by standard breeding regimen. As published elsewhere, in B6;129S1-Tg(Myh7-Cre)^{1Jmk} mice, the Cre enzyme has a significant activity at embryonic day 17.5 (Oka et al., 2006). Finally, female *Fgf23*^{fl/fl}/*Myh7-cre*⁻ mice were bred with males fully recombined for *Fgf23* (*Fgf23*^{fl/fl}/*Myh7-cre*⁺). To verify genotypes, PCR products were amplified from genomic DNA using primer pairs spanning the floxed exon 2 region of murine *Fgf23* and Cre recombinase in a semi-quantitative multiplex PCR (see Methods). Thereby a 253 bp product represented the wild-type *Fgf23* allele, a 367 bp product the floxed *Fgf23* allele, and a 550 bp product the Cre expression (Figure 2B). Male and female *Fgf23*^{fl/fl}/*Myh7-cre*⁺ mice (in the following termed as *Fgf23*^{fl/fl}/*cre*⁺) were analyzed in all



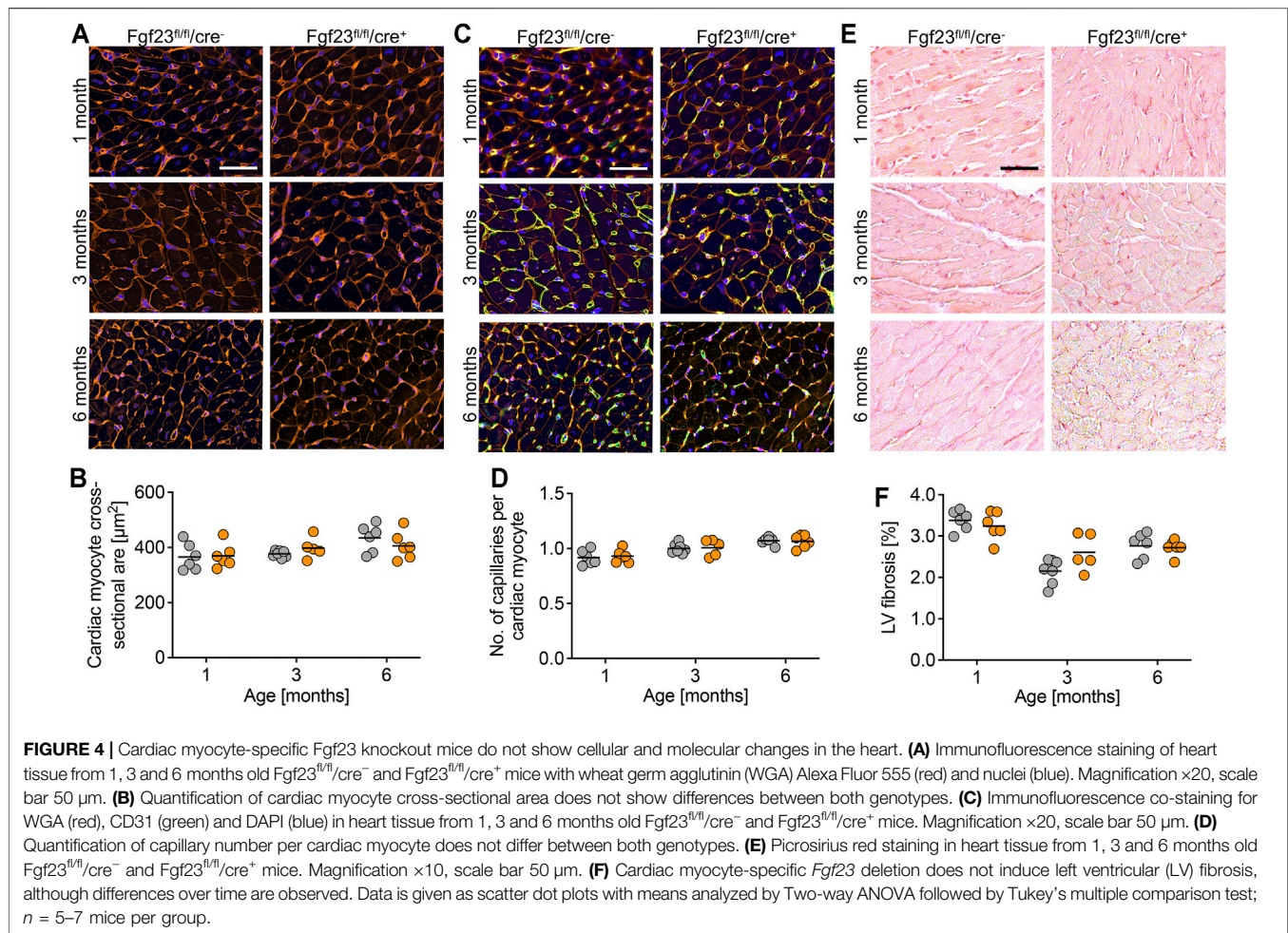
experiments and respective non-recombined *Fgf23^{fl/fl}/Myh7-cre⁻* littermates (in the following termed as *Fgf23^{fl/fl}/cre⁻*) were used as controls. First, we verified the cardiac myocyte-specific *Fgf23* knockout. Thereby, *Fgf23^{fl/fl}/cre⁺* mice showed significantly reduced cardiac *Fgf23* mRNA expression compared to controls (**Figure 2C**), while their osseous *Fgf23* synthesis remained unaffected (**Figure 2D**). Western blot analysis showed significantly reduced full-length cardiac *Fgf23* protein in *Fgf23^{fl/fl}/cre⁺* compared to control mice (**Figure 2E**). Using anti- α -Actinin antibody, immunofluorescence microscopy confirmed the cardiac myocytes-specific *Fgf23* knockout (**Figure 2F**). However, circulating total and intact *Fgf23* (i*Fgf23*) levels in *Fgf23^{fl/fl}/cre⁺* mice were comparable to controls (**Figures 2G,H**), and phosphate and calcium metabolism remained unchanged up to six months of age (**Supplementary Table S2**).

Cardiac Myocyte-specific *Fgf23* Deletion Does Not Affect Cardiac Function or Structure in Unchallenged Mice

Mice with cardiac myocyte specific *Fgf23* deletion showed normal body length and heart size compared to age-matched controls (**Figure 3A**). The body weight related organ weights including heart, lung, kidney and liver increased with age, but did not differ between both genotypes (**Supplementary Table S3**). However, the mortality of *Fgf23^{fl/fl}/cre⁺* mice during the first 6 months of

life was slightly but significantly increased compared to controls (**Figure 3B**). Next, we performed echocardiography and Millar catheter to determine whether cardiac function was affected in *Fgf23^{fl/fl}/cre⁺* mice, which in turn may promote their increased mortality. In echocardiography, no differences between *Fgf23^{fl/fl}/cre⁻* and *Fgf23^{fl/fl}/cre⁺* mice were observed, irrespective of age (**Figure 3C**, **Supplementary Table S4**), except for a significantly reduced end-systolic volume (ESV) and slightly lower end-diastolic volume (EDV) in six months old *Fgf23^{fl/fl}/cre⁺* mice compared to control (**Figures 3D,E**). Using Millar catheter, no differences were found in end-systolic or end-diastolic LV pressure or stroke work (**Figures 3F,G**). Overall, these data indicate no pathologic cardiac phenotype in *Fgf23^{fl/fl}/cre⁺* mice.

Next, we performed histological analyses to determine alterations in the cardiac structure of *Fgf23^{fl/fl}/cre⁺* and control mice. Quantified by wheat germ agglutinin (WGA) staining and fluorescence microscopy, cardiac myocyte cross-sectional area did not differ between the genotypes (**Figures 4A,B**). This was in line with the equal expression of the pro-hypertrophic markers atrial natriuretic peptide (*ANP*), brain natriuretic peptide (*BNP*) and beta myosin heavy chain (*bmHC*) in *Fgf23^{fl/fl}/cre⁺* mice compared to controls, irrespective of age (**Supplementary Figures S1A–C**). Neither the capillary density (**Figures 4C,D**) nor the accumulation of interstitial collagen fibers (**Figures 4E,F**) were affected by the conditional cell-specific disruption of *Fgf23* in cardiac myocytes over time. The mRNA expression of the profibrotic marker transforming growth factor beta 1 (*Tgfb1*) and its

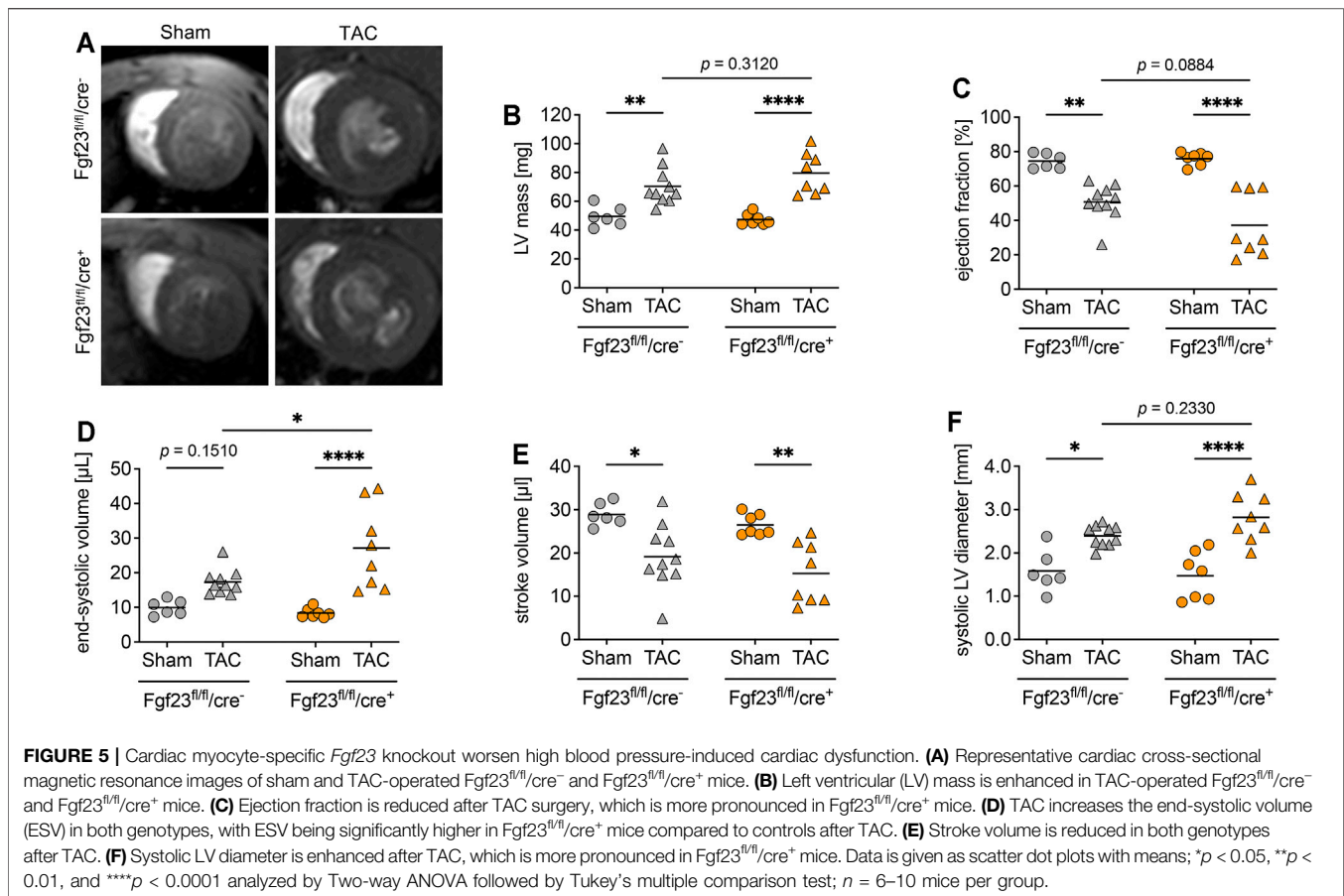


downstream target connective tissue growth factor (*Ctgf*) was equal between both groups (**Supplementary Figures S1D,E**). Consistently, collagen type 1, alpha 1, recently identified as a marker in human heart failure progression related to tissue fibrosis (Hua et al., 2020) and encoded by the gene *Colla1*, was not differentially expressed in *Fgf23^{fl/fl}/cre⁺* mice compared to age-matched controls (**Supplementary Figure S1F**). Thus, in line with normal heart function in echocardiography and Millar catheter, conditional deletion of *Fgf23* in cardiac myocytes does not alter cardiac structure.

Loss of Cardiac Myocyte-specific *Fgf23* Does Not Alter Impaired Cardiac Function After Transverse Aortic Constriction

Enhanced circulating and cardiac FGF23 levels are shown to be associated with LVH in CKD (Faul et al., 2011; Leifheit-Nestler et al., 2016). Furthermore, high plasma FGF23 is present in patients with infarction-related cardiogenic shock and acute decompensated heart failure, which is associated with disease severity and mortality (Pöss et al., 2013; Fuernau et al., 2014; Andersen et al., 2016). It was previously shown that TAC, a

model for high blood pressure-induced cardiac hypertrophy and heart failure, induces the expression of cardiac *Fgf23* in mice (Slavic et al., 2017). Thus, we next investigated whether the deletion of cardiac myocyte-specific *Fgf23* is protective against pathological cardiac remodeling after aortic banding. Two weeks after TAC, cardiac function and geometry were determined by magnetic resonance imaging (MRI) (**Figure 5A**). TAC significantly enhanced LV mass and impaired ejection fraction (EF) in both genotypes (**Figures 5B,C**). It increased ESV, decreased stroke volume (SV) and enlarged systolic LV diameter in both groups (**Figures 5D-F**). Compared to respective TAC *Fgf23^{fl/fl}/cre⁻* controls, heart function seemed to be even more impaired in TAC-operated *Fgf23^{fl/fl}/cre⁺* mice. However, H&E-stained cardiac mid chamber cross-sections revealed increased LV wall thickness after TAC in both groups (**Figure 6A**). Concomitantly, similar increases in cardiac myocyte size and pro-hypertrophic *BNP* mRNA expression were seen in *Fgf23^{fl/fl}/cre⁺* mice and controls after TAC (**Figures 6B-D**). The mean percentage of LV fibrosis after TAC was similar in *Fgf23^{fl/fl}/cre⁺* and *Fgf23^{fl/fl}/cre⁻* mice (**Figures 6E,F**). Taken together, our findings suggest that specific disruption of *Fgf23* in cardiac myocytes does not



essentially alter cardiac dysfunction in the TAC mouse model, with the exception of a modest alteration in ESV that however, does not translate to any changes in hypertrophy, fibrosis or chamber remodeling.

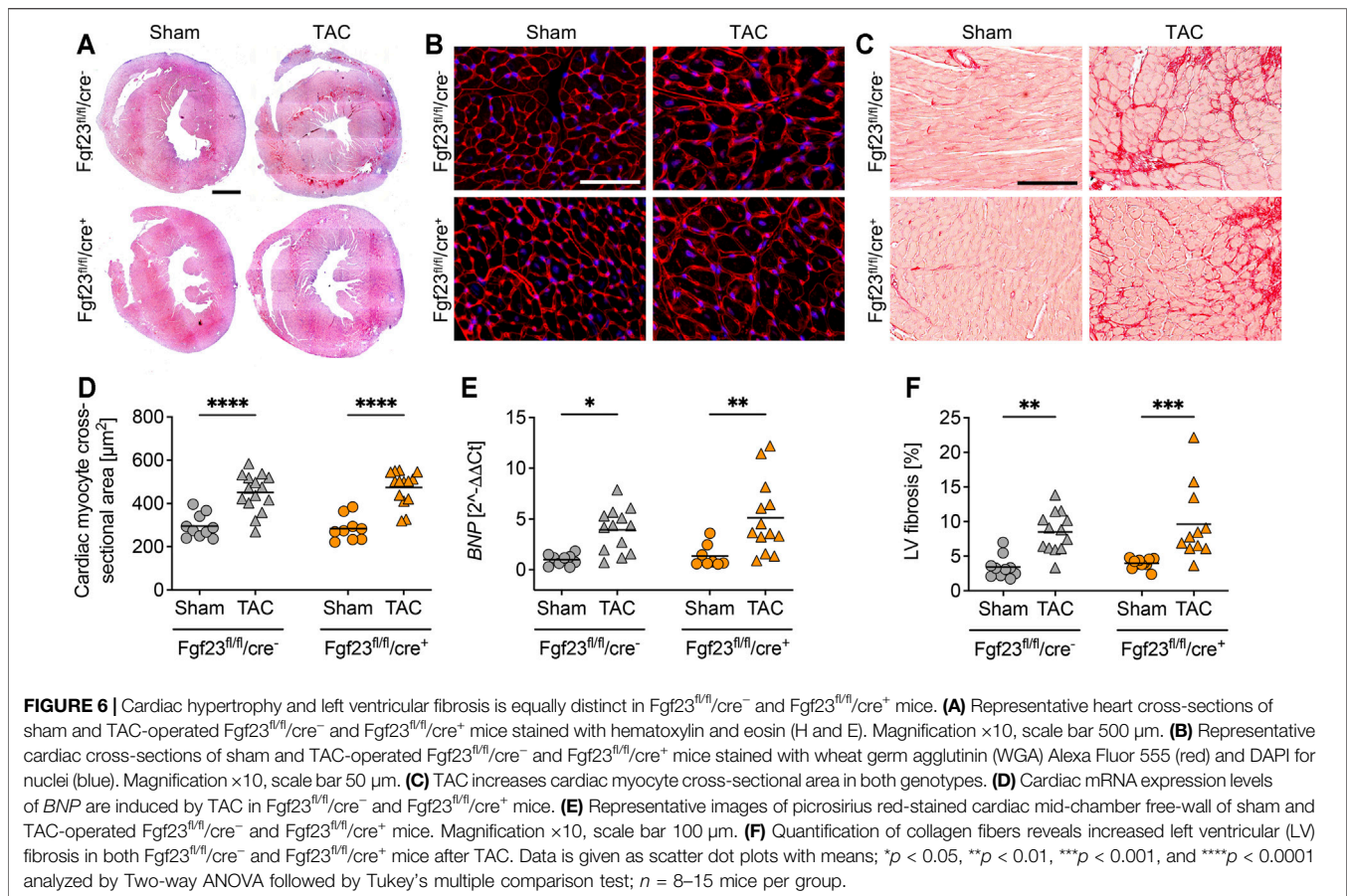
Transverse Aortic Constriction Induces the Expression of *Fgf23* in Cardiac Fibroblasts and Endothelial Cells

Next, we assessed the TAC-induced changes in *Fgf23* synthesis. As shown by qPCR analysis, TAC stimulated the expression of *Fgf23* in bone of both *Fgf23^{fl/fl}/cre⁺* mice and *Fgf23^{fl/fl}/cre⁻* mice, although the latter did not reach the level of statistical significance in Two-way ANOVA comparisons (**Figure 7A**). TAC further resulted in increased *Fgf23* mRNA levels in *Fgf23^{fl/fl}/cre⁻* mice using total cardiac tissue (**Figure 7B**). Interestingly, cardiac *Fgf23* was also slightly increased after TAC in *Fgf23^{fl/fl}/cre⁺* mice compared to sham, although *Fgf23* mRNA levels were significantly lower than in TAC-operated controls. To elucidate the origin of TAC-induced cardiac *Fgf23*, we next performed co-immunofluorescence staining of *Fgf23* with α -Actinin, PDGFR α , and CD31. TAC did not affect the synthesis of *Fgf23* in cardiac myocytes (**Figure 7C**), while PDGFR α co-staining revealed enhanced accumulation of cardiac fibroblasts clearly expressing *Fgf23* in both genotypes

(**Figure 7D**), which was in line with severe fibrosis due to TAC as detected by picrosirius red staining (**Figures 6E,F**). Interestingly, TAC caused an enhanced *Fgf23* synthesis in endothelial cells in both genotypes, as shown by increased *Fgf23* detection in CD31-positive blood vessels (**Figure 7E**). The isolation of cardiac myocytes, cardiac fibroblasts and endothelial cells confirmed a specific induction of *Fgf23* transcription in cardiac fibroblasts and endothelial cells after TAC compared to sham, while the absolute *Fgf23* levels in cardiac myocytes remained unchanged (**Figure 7F**). Taken together, irrespective of the disruption of cardiac myocyte-specific *Fgf23*, TAC leads to increased cardiac *Fgf23* levels that most likely results from a specific induction of *Fgf23* synthesis in cardiac fibroblasts and endothelial cells.

DISCUSSION

Enhanced FGF23 levels are associated with the development of LVH in patients with CKD (Kovesdy and Quarles, 2016) and it has been shown that FGF23 directly induces cardiac hypertrophy *in vitro* and *in vivo* (Faul et al., 2011). Here we showed that the healthy heart is a source of *Fgf23*, where cardiac myocytes, fibroblasts and endothelial cells express *Fgf23*. Although, a cardiac myocyte-specific *Fgf23* knockout in mice did neither resulted in altered mineral metabolism, nor in cardiac

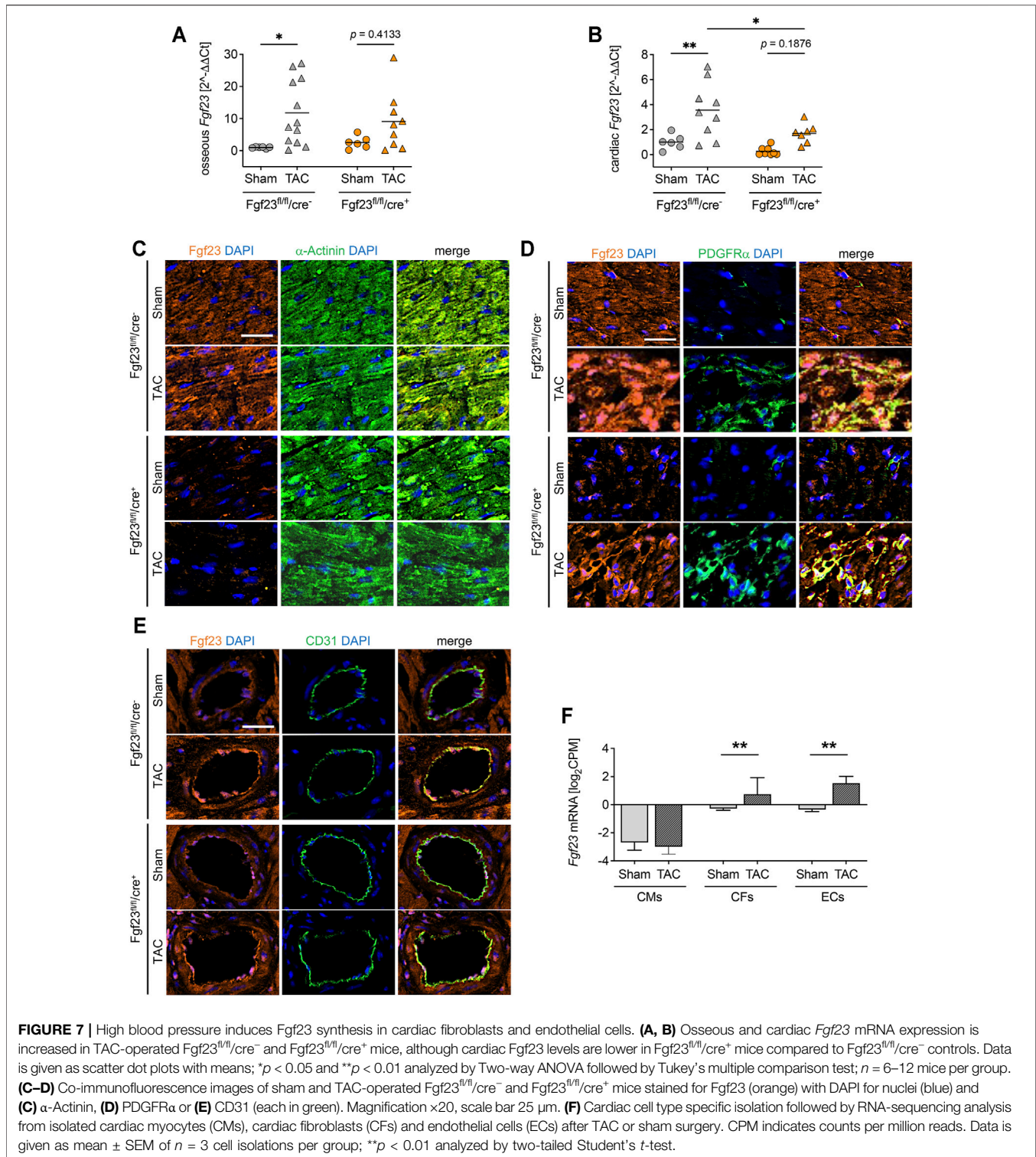


dysfunction or cellular pathologies, overall mortality was enhanced in $Fgf23^{fl/fl}/cre^{+}$ mice within six months of age. After TAC, cardiac function deteriorated in $Fgf23^{fl/fl}/cre^{+}$ and $Fgf23^{fl/fl}/cre^{-}$ mice compared to sham controls and the evaluation of cardiac *Fgf23* synthesis revealed elevated expression in cardiac fibroblasts and endothelial cells after TAC even in $Fgf23^{fl/fl}/cre^{+}$ mice. Interestingly, cardiac myocyte-derived *Fgf23* was unaffected by TAC.

High intra-cardiac synthesis of FGF23 has been shown in patients with CKD and LVH (Leifheit-Nestler et al., 2016) as well as in animal models of experimental uremia (Leifheit-Nestler et al., 2017), myocardial infarction (Andrukhova et al., 2015; Schumacher et al., 2019) and after pulmonary artery banding (Kuga et al., 2020). It is well established that FGF23 induces LVH (Faul et al., 2011), and we and others have shown that cardiac myocytes express FGF23 *in vitro* and in human heart samples (Richter et al., 2015; Leifheit-Nestler et al., 2016; Leifheit-Nestler and Haffner, 2018). Indeed, most investigations regarding cardiac FGF23 focused on the LV and associated disorders, but here we observed that also the right ventricle is a source of *Fgf23* in healthy mice. This was supported by a recently published study of Kuga et al. showing that *Fgf23* promoted cardiac fibrosis in the right ventricle, predominantly mediated by the induction in cardiac myocytes (Kuga et al., 2020). FGF23 was further shown to be expressed in human coronary arteries of patients with kidney function impairment (Van Venrooij et al., 2014)

underscoring our findings on the expression of *Fgf23* in healthy mouse endothelium in the present study. However, the regulation of endogenous FGF23 synthesis in cardiac endothelial cells has not been addressed so far. The expression of FGF23 in cardiac fibroblasts is controversial. Here, we showed a clear expression of *Fgf23* in cardiac fibroblasts of healthy mice, whereas Schumacher et al. found *Fgf23* to be expressed by cardiac fibroblasts only immediately after myocardial infarction (MI) during the inflammatory phase, but neither in later phases nor in health (Schumacher et al., 2019). Hao et al. were able to detect *Fgf23* expression in untreated adult mouse cardiac fibroblasts (AMCF) as well as in neonatal rat cardiac fibroblasts (NRCF) *in vitro* (Hao et al., 2016), whereas others could not detect *Fgf23* in NRCF (Leifheit-Nestler et al., 2018). However, *Fgf23* was also detected in kidney fibroblasts, especially myofibroblasts (Smith et al., 2017). Additionally, Smith et al. pointed out that *Fgf23* was induced in kidney fibroblasts after injury, which appears to be in line with the findings of Schumacher et al. regarding the induction of *Fgf23* in cardiac fibroblasts after MI (Schumacher et al., 2019) and our finding of increased *Fgf23* expression in cardiac fibroblasts after TAC.

Whether different diseases stimulate cardiac FGF23 synthesis or *vice versa* high cardiac FGF23 promotes these cardiac pathologies is still not clear and the specific cellular source of cardiac FGF23 in these settings has not been sufficiently investigated. Genetically modified animal models are



important to study and understand the function of specific genes in health and disease. Hereby, mouse models with deletion or overexpression of *Fgf23* were critical for understanding the role of *Fgf23* in the bone-kidney signaling axis (Shimada et al., 2004a and

Shimada et al., 2004b). At birth, transgenic *Fgf23* overexpressing mice and global *Fgf23* knockout mice are phenotypically not different from wild-type mice, but develop growth retardation due to skeletal malformations at weaning age or by 13 days of age,

respectively. Although both genotypes are viable, global *Fgf23* knockout mice did not survive longer than 13 weeks of age (Shimada et al., 2004b). Therefore, we generated a mouse model with conditional cardiac myocyte-specific *Fgf23* knockout to investigate the role of cardiac FGF23 in health and disease. We confirmed that the cardiac mRNA expression of *Fgf23* in *Fgf23^{fl/fl}/cre⁺* was almost undetectable and histological evaluation revealed no synthesis in cardiac myocytes. *Fgf23* protein levels in whole heart tissue lysates were reduced compared to controls but still present. This could be due to unchanged *Fgf23* concentrations in cardiac fibroblasts and endothelial cells. Compared to the global *Fgf23* knockout mouse, *Fgf23^{fl/fl}/cre⁺* mice were also viable but did not show any growth retardation at birth or in later stages of life, which can be attributed to the normal bone and mineral metabolism. Heart geometry and function was not altered in mice with conditional cardiac myocyte-specific *Fgf23* disruption up to six months of age. Comparably, *Fgf23^{fl/fl}/cre⁺* mice showed no structural or molecular cardiac abnormalities.

Clinical studies regarding the association of high FGF23 and hypertension are controversial (Li et al., 2018; Ramezanzade et al., 2019; Drew et al., 2020). Nevertheless, *in vivo* studies showed that *Fgf23* increased sodium uptake in the distal tubule resulting in volume expansion, hypertension and finally cardiac hypertrophy (Andrukhova et al., 2014). In addition, TAC-induced LVH in mice was associated with increased cardiac *Fgf23* in whole tissue samples (Slavic et al., 2017; Matsui et al., 2018). Slavic et al. performed TAC in a global *Fgf23* knockout mouse crossed with mice expressing a non-functioning vitamin D receptor (VDR) to prohibit vitamin D intoxication on a rescue diet to ensure normal growth, and showed no differences in the progression of cardiac hypertrophy compared to controls (Slavic et al., 2017). However, effects of non-functioning VDR or rescue diet cannot be excluded in this model and do not refute a possible causal relationship of cardiac FGF23 and pressure-induced LVH. Taken all these into account, it cannot be ruled out that loss of FGF23 in cardiac myocytes protects them from hypertrophic growth or at least reduces pro-hypertrophic signaling. To analyze whether cardiac FGF23 plays a role in pressure-induced LVH, we performed TAC on *Fgf23^{fl/fl}/cre⁺* and control mice. In contrast to Slavic et al., TAC even tended to worsen cardiac function in *Fgf23^{fl/fl}/cre⁺*, although this was not translated to any alterations in cellular hypertrophy, fibrosis or chamber remodeling. Analyzing cardiac *Fgf23* in more detail, our data observed increased *Fgf23* mRNA expression due to TAC even in total heart tissue of cardiac myocyte-specific *Fgf23* knockout mice. Immunofluorescence staining of cardiac mid-chamber cross-sections and deep-sequencing data of isolated adult cardiac myocytes, cardiac fibroblasts and endothelial cells revealed a specific induction of *Fgf23* synthesis in cardiac fibroblasts and endothelial cells after TAC, which explain enhanced *Fgf23* expression even in TAC-operated hearts of

Fgf23^{fl/fl}/cre⁺ mice. Taken all this into account, cardiac myocyte specific depletion of *Fgf23* might not have a great impact in heart performance and structure at both basal and after stressing conditions due to the expression in other cardiac cell types. Additionally, enhanced expression and secretion of cardiac fibroblast-derived *Fgf23* may stimulate myofibroblast differentiation and promote hypertrophic growth of cardiac myocytes in an endocrine manner even in *Fgf23^{fl/fl}/cre⁺* mice after TAC. The deleterious effect of high *Fgf23* on the endothelium has also been discussed before (Six et al., 2014; Silswal N et al., 2014; Verkaik et al., 2018; Richter et al., 2016). Thus, *Fgf23* secreted from cardiac fibroblast may further affect endothelial cells in *Fgf23^{fl/fl}/cre⁺* mice in a paracrine manner that are already under stress due to high pressure after TAC. Crosstalk between endothelial cells and cardiac myocytes is also known and intensively studied (Chen et al., 2010; Zhang et al., 2015; Kivelä et al., 2019). Here, we showed that *Fgf23* synthesis was induced in endothelial cells in *Fgf23^{fl/fl}/cre⁺* and control mice after TAC compared to respective sham-operated animals, which could further strengthen cardiac myocytes hypertrophy irrespective of cardiac myocyte-derived *Fgf23*.

Taken together, we showed that besides the LV, FGF23 is also expressed in the right ventricle and thus, beside LVH, could play a role in other cardiac diseases. Our data further point out that FGF23 is not only expressed in cardiac myocytes but also in cardiac fibroblasts and endothelial cells and thereby may impact heart development, and physiological and pathological cardiac function. Additionally, we investigated for the first-time cell type-specific regulation of FGF23 in heart tissue due to high blood pressure showing increased synthesis in cardiac fibroblasts and endothelial cells. Exact molecular mechanisms and the crosstalk between cardiac myocytes and non-cardiac myocytes with respect to FGF23 and its impact for cardiac physiology and pathology have to be addressed in respective *in vivo* and *in vitro* settings in further studies.

DATA AVAILABILITY STATEMENT

The original contributions presented in the study are included in the article/**Supplementary Material**. Further inquiries can be directed to the corresponding author.

ETHICS STATEMENT

All experimental animal procedures were performed in accordance with national animal protection guidelines from Directive 2010/63/EU of the European Parliament on the protection of animals used for scientific purposes and approved by the governmental committee on animal welfare Lower Saxony (Niedersächsische Landesamt für Verbraucherschutz und Lebensmittelsicherheit; #15/1912).

AUTHOR CONTRIBUTIONS

ML-N. and DH conceived and designed the study. FE, BR, SS, IV and AG performed experiments and analyzed data. MS performed TAC surgery. JH provided the Myh7-cre mice and discussed breeding strategies. JH, TT and DH supported funding and provided infrastructure. FE and BR drafted the manuscript. ML-N and DH critically revised the paper. All authors approved the final version of the manuscript.

FUNDING

This work was supported with internal funding.

REFERENCES

- Andersen, I. A., Huntley, B. K., Sandberg, S. S., Heublein, D. M., and Burnett, J. C. (2016). Elevation of Circulating but Not Myocardial FGF23 in Human Acute Decompensated Heart Failure. *Nephrol. Dial. Transpl.* 31, 767–772. doi:10.1093/ndt/gfv398
- Andrukhova, O., Slavic, S., Smorodchenko, A., Zeitz, U., Shalhoub, V., and Lanske, B. (2014). FGF23 Regulates Renal Sodium Handling and Blood Pressure. *EMBO Mol. Med.* 6, 744–759. doi:10.1002/emmm.201303716
- Andrukhova, O., Slavic, S., Odörfer, K. I., and Erben, R. G. (2015). Experimental Myocardial Infarction Upregulates Circulating Fibroblast Growth Factor-23. *J. Bone Miner. Res.* 30, 1831–1839. doi:10.1002/jbmr.2527
- Appari, M., Breitbart, A., Brandes, F., Szaroszyk, M., Froese, N., Korf-Klingebiel, M., et al. (2017). C1q-TNF-Related Protein-9 Promotes Cardiac Hypertrophy and Failure. *Circ. Res.* 120, 66–77. doi:10.1161/circresaha.116.309398
- Böckmann, I., Lischka, J., Richter, B., Deppe, J., Rahn, A., Fischer, D.-C., et al. (2019). FGF23-mediated Activation of Local RAAS Promotes Cardiac Hypertrophy and Fibrosis. *Ijms* 20, 4634. doi:10.3390/ijms20184634
- Chen, K., Bai, H., Arzigian, M., Gao, Y.-X., Bao, J., Wu, W.-S., et al. (2010). Endothelial Cells Regulate Cardiomyocyte Development from Embryonic Stem Cells. *J. Cel. Biochem.* 111, 29–39. doi:10.1002/jcb.22680
- De Borst, M. H., Vervloet, M. G., Ter Wee, P. M., and Navis, G. (2011). Cross Talk between the Renin-Angiotensin-Aldosterone System and Vitamin D-FGF-23-Klotho in Chronic Kidney Disease: Figure 1. *Jasn* 22, 1603–1609. doi:10.1681/asn.2010121251
- Drew, D. A., Katz, R., Kritchevsky, S., Ix, J. H., Shlipak, M. G., Newman, A. B., et al. (2020). Fibroblast Growth Factor 23 and Blood Pressure in Older Adults: The Health, Aging, and Body Composition Study. *Hypertension* 76, 236–243. doi:10.1161/hypertensionaha.120.14703
- Eckardt, K.-U., Coresh, J., Devuyst, O., Johnson, R. J., Köttgen, A., Levey, A. S., et al. (2013). Evolving Importance of Kidney Disease: From Subspecialty to Global Health burden. *The Lancet* 382, 158–169. doi:10.1016/s0140-6736(13)60439-0
- Faul, C., Amaral, A. P., Oskouei, B., Hu, M.-C., Sloan, A., Isakova, T., et al. (2011). FGF23 Induces Left Ventricular Hypertrophy. *J. Clin. Invest.* 121, 4393–4408. doi:10.1172/jci46122
- Fischer, D.-C., Mischek, A., Wolf, S., Rahn, A., Salweski, B., Kundt, G., et al. (2012). Paediatric Reference Values for the C-Terminal Fragment of Fibroblast-Growth Factor-23, Sclerostin, Bone-specific Alkaline Phosphatase and Isoform 5b of Tartrate-Resistant Acid Phosphatase. *Ann. Clin. Biochem.* 49, 546–553. doi:10.1258/acb.2012.011274
- Fon Tacer, K., Bookout, A. L., Ding, X., Kurosu, H., John, G. B., Wang, L., et al. (2010). Research Resource: Comprehensive Expression Atlas of the Fibroblast Growth Factor System in Adult Mouse. *Mol. Endocrinol.* 24, 2050–2064. doi:10.1210/me.2010-0142
- Fuernau, G., Pöss, J., Denks, D., Desch, S., Heine, G. H., Eitel, I., et al. (2014). Fibroblast Growth Factor 23 in Acute Myocardial Infarction Complicated by Cardiogenic Shock: A Biomarker Substudy of the Intraaortic Balloon Pump in

ACKNOWLEDGMENTS

The authors would like to thank Karina Zimmer for performing echocardiography, Margit Überheide for technical support, and the core facility of the Small Animal Imaging Center, Hannover Medical School, for performing MRI.

SUPPLEMENTARY MATERIAL

The Supplementary Material for this article can be found online at: <https://www.frontiersin.org/articles/10.3389/fcell.2021.791479/full#supplementary-material>

- Cardiogenic Shock II (IABP-SHOCK II) Trial. *Crit. Care* 18, 713. doi:10.1186/s13054-014-0713-8
- Go, A. S., Chertow, G. M., Fan, D., McCulloch, C. E., and Hsu, C.-y. (2004). Chronic Kidney Disease and the Risks of Death, Cardiovascular Events, and Hospitalization. *N. Engl. J. Med.* 351, 1296–1305. doi:10.1056/nejmoa041031
- Grabner, A., Amaral, A. P., Schramm, K., Singh, S., Sloan, A., Yanucil, C., et al. (2015). Activation of Cardiac Fibroblast Growth Factor Receptor 4 Causes Left Ventricular Hypertrophy. *Cel. Metab.* 22, 1020–1032. doi:10.1016/j.cmet.2015.09.002
- Grund, A., Szaroszyk, M., Korf-Klingebiel, M., Malek Mohammadi, M., Trogisch, F. A., Schrameck, U., et al. (2019a). TIP30 Counteracts Cardiac Hypertrophy and Failure by Inhibiting Translational Elongation. *EMBO Mol. Med.* 11, e10018. doi:10.15252/emmm.201810018
- Grund, A., Szaroszyk, M., Döppner, J. K., Malek Mohammadi, M., Kattih, B., Korf-Klingebiel, M., et al. (2019b). A Gene Therapeutic Approach to Inhibit Calcium and Integrin Binding Protein 1 Ameliorates Maladaptive Remodelling in Pressure Overload. *Cardiovasc. Res.* 115, 71–82. doi:10.1093/cvr/cvy154
- Gutierrez, O., Isakova, T., Rhee, E., Shah, A., Holmes, J., Collerone, G., et al. (2005). Fibroblast Growth Factor-23 Mitigates Hyperphosphatemia but Accentuates Calcitriol Deficiency in Chronic Kidney Disease. *Jasn* 16, 2205–2215. doi:10.1681/asn.2005010052
- Ham, O., Jin, W., Lei, L., Huang, H. H., Tsuji, K., Huang, M., et al. (2018). Pathological Cardiac Remodeling Occurs Early in CKD Mice from Unilateral Urinary Obstruction, and Is Attenuated by Enalapril. *Sci. Rep.* 8, 16087. doi:10.1038/s41598-018-34216-x
- Hao, H., Li, X., Li, Q., Lin, H., Chen, Z., Xie, J., et al. (2016). FGF23 Promotes Myocardial Fibrosis in Mice through Activation of β -catenin. *Oncotarget* 7, 64649–64664. doi:10.18632/oncotarget.11623
- Hausler, M. R., Whitfield, G. K., Kaneko, I., Forster, R., Saini, R., Hsieh, J.-C., et al. (2012). The Role of Vitamin D in the FGF23, Klotho, and Phosphate Bone-Kidney Endocrine axis. *Rev. Endocr. Metab. Disord.* 13, 57–69. doi:10.1007/s11154-011-9199-8
- Heineke, J., Auger-Messier, M., Xu, J., Oka, T., Sargent, M. A., York, A., et al. (2007). Cardiomyocyte GATA4 Functions as a Stress-Responsive Regulator of Angiogenesis in the Murine Heart. *J. Clin. Invest.* 117, 3198–3210. doi:10.1172/jci32573
- Hua, X., Wang, Y. Y., Jia, P., Xiong, Q., Hu, Y., Chang, Y., et al. (2020). Multi-level Transcriptome Sequencing Identifies COL1A1 as a Candidate Marker in Human Heart Failure Progression. *BMC Med.* 18, 2–16. doi:10.1186/s12916-019-1469-4
- Kawata, T., Imanishi, Y., Kobayashi, K., Miki, T., Arnold, A., Inaba, M., et al. (2007). Parathyroid Hormone Regulates Fibroblast Growth Factor-23 in a Mouse Model of Primary Hyperparathyroidism. *Jasn* 18, 2683–2688. doi:10.1681/asn.2006070783
- Kestenbaum, B., Sachs, M. C., Hoofnagle, A. N., Siscovick, D. S., Ix, J. H., Robinson-Cohen, C., et al. (2014). Fibroblast Growth Factor-23 and Cardiovascular Disease in the General Population. *Circ. Heart Fail.* 7, 409–417. doi:10.1161/circheartfailure.113.000952

- Kivelä, R., Hemanthakumar, K. A., Vaparanta, K., Robciuc, M., Izumiya, Y., Kidoya, H., et al. (2019). Endothelial Cells Regulate Physiological Cardiomyocyte Growth via VEGFR2-Mediated Paracrine Signaling. *Circulation* 139, 2570–2584. doi:10.1161/circulationaha.118.036099
- Kovesdy, C. P., and Quarles, L. D. (2016). FGF23 from Bench to Bedside. *Am. J. Physiology-Renal Physiol.* 310, F1168–F1174. doi:10.1152/ajprenal.00606.2015
- Kuga, K., Kusakari, Y., Uesugi, K., Semba, K., Urashima, T., Akaike, T., et al. (2020). Fibrosis Growth Factor 23 Is a Promoting Factor for Cardiac Fibrosis in the Presence of Transforming Growth Factor-B1. *PLoS One* 15, e0231905. doi:10.1371/journal.pone.0231905
- Leifheit-Nestler, M., Grabner, A., Hermann, L., Richter, B., Schmitz, K., Fischer, D.-C., et al. (2017). Vitamin D Treatment Attenuates Cardiac FGF23/FGFR4 Signaling and Hypertrophy in Uremic Rats. *Nephrol. Dial. Transpl.* 32, 1493–1503. doi:10.1093/ndt/gfw454
- Leifheit-Nestler, M., große Siemer, R., Flasbart, K., Richter, B., Kirchhoff, F., Ziegler, W. H., et al. (2016). Induction of Cardiac FGF23/FGFR4 Expression Is Associated with Left Ventricular Hypertrophy in Patients with Chronic Kidney Disease. *Nephrol. Dial. Transpl.* 31, 1088–1099. doi:10.1093/ndt/gfv421
- Leifheit-Nestler, M., and Haffner, D. (2018). Paracrine Effects of FGF23 on the Heart. *Front. Endocrinol.* 9, 278. doi:10.3389/fendo.2018.00278
- Leifheit-Nestler, M., Kirchhoff, F., Nespore, J., Richter, B., Soetje, B., Klintschar, M., et al. (2018). Fibroblast Growth Factor 23 Is Induced by an Activated Renin-Angiotensin-Aldosterone System in Cardiac Myocytes and Promotes the Pro-fibrotic Crosstalk between Cardiac Myocytes and Fibroblasts. *Nephrol. Dial. Transpl.* 33, 1722–1734. doi:10.1093/ndt/gfy006
- Li, J. X., Yu, G. Q., and Zhuang, Y. Z. (2018). Impact of Serum FGF23 Levels on Blood Pressure of Patients with Chronic Kidney Disease. *Eur. Rev. Med. Pharmacol. Sci.* 22, 721–725. doi:10.26355/eurrev_201802_14299
- Lutsey, P. L., Alonso, A., Selvin, E., Pankow, J. S., Michos, E. D., Agarwal, S. K., et al. (2014). Fibroblast Growth Factor-23 and Incident Coronary Heart Disease, Heart Failure, and Cardiovascular Mortality: The Atherosclerosis Risk in Communities Study. *J. Am. Heart Assoc.* 3, e000936. doi:10.1161/JAHA.114.000936
- Matsui, I., Oka, T., Kusunoki, Y., Mori, D., Hashimoto, N., Matsumoto, A., et al. (2018). Cardiac Hypertrophy Elevates Serum Levels of Fibroblast Growth Factor 23. *Kidney Int.* 94, 60–71. doi:10.1016/j.kint.2018.02.018
- Oka, T., Maillet, M., Watt, A. J., Schwartz, R. J., Aronow, B. J., Duncan, S. A., et al. (2006). Cardiac-specific Deletion of Gata4 Reveals its Requirement for Hypertrophy, Compensation, and Myocyte Viability. *Circ. Res.* 98, 837–845. doi:10.1161/01.res.0000215985.18538.c4
- Paoletti, E., De Nicola, L., Gabbai, F. B., Chiodini, P., Ravera, M., Pieracci, L., et al. (2016). Associations of Left Ventricular Hypertrophy and Geometry with Adverse Outcomes in Patients with CKD and Hypertension. *Cjasn* 11, 271–279. doi:10.2215/cjn.06980615
- Pöss, J., Mahfoud, F., Seiler, S., Heine, G. H., Fliser, D., Böhm, M., et al. (2013). FGF-23 Is Associated with Increased Disease Severity and Early Mortality in Cardiogenic Shock. *Eur. Heart J. Acute Cardiovasc. Care* 2, 211–218. doi:10.1177/2048872613494025
- Ramezanzade, E., Minoof, F., Lebad, M. K., Jedinia, A., Saheli, Y. H., Aghajanzadeh, P., et al. (2019). Investigating the Relationship between Blood Pressure and Serum FGF23 Level in Patients Undergoing Hemodialysis in Guilan Province, A Cross Sectional Study. *Iran J. Kidney Dis.* 13, 262–268.
- Richter, B., Haller, J., Haffner, D., and Leifheit-Nestler, M. (2016). Klotho Modulates FGF23-Mediated NO Synthesis and Oxidative Stress in Human Coronary Artery Endothelial Cells. *Pflugers Arch. - Eur. J. Physiol.* 468, 1621–1635. doi:10.1007/s00424-016-1858-x
- Richter, M., Lautze, H.-J., Walther, T., Braun, T., Kostin, S., and Kubin, T. (2015). The Failing Heart Is a Major Source of Circulating FGF23 via Oncostatin M Receptor Activation. *J. Heart Lung Transplant.* 34, 1211–1214. doi:10.1016/j.healun.2015.06.007
- Riminucci, M., Collins, M. T., Fedarko, N. S., Cherman, N., Corsi, A., White, K. E., et al. (2003). FGF-23 in Fibrous Dysplasia of Bone and its Relationship to Renal Phosphate Wasting. *J. Clin. Invest.* 112, 683–692. doi:10.1172/JCI18399
- Rodríguez-Ortiz, M. E., Lopez, I., Muñoz-Castañeda, J. R., Martínez-Moreno, J. M., Ramírez, A. P., Pineda, C., et al. (2012). Calcium Deficiency Reduces Circulating Levels of FGF23. *Jasn* 23, 1190–1197. doi:10.1681/asn.2011101006
- Sarnak, M. J., Levey, A. S., Schoolwerth, A. C., Coresh, J., Culleton, B., Hamm, L. L., et al. (2003). Kidney Disease as a Risk Factor for Development of Cardiovascular Disease. *Circulation* 108, 2154–2169. doi:10.1161/01.cir.0000095676.90936.80
- Schumacher, D., Alampour-Rajabi, S., Ponomarev, V., Curaj, A., Wu, Z., Staudt, M., et al. (2019). Cardiac FGF23: New Insights into the Role and Function of FGF23 after Acute Myocardial Infarction. *Cardiovasc. Pathol.* 40, 47–54. doi:10.1016/j.carpath.2019.02.001
- Shimada, T., Hasegawa, H., Yamazaki, Y., Muto, T., Hino, R., Takeuchi, Y., et al. (2004). FGF-23 Is a Potent Regulator of Vitamin D Metabolism and Phosphate Homeostasis. *J. Bone Miner. Res.* 19, 429–435. doi:10.1359/JBMR.0301264
- Shimada, T., Yamazaki, Y., Takahashi, M., Hasegawa, H., Urakawa, I., Oshima, T., et al. (2005). Vitamin D Receptor-independent FGF23 Actions in Regulating Phosphate and Vitamin D Metabolism. *Am. J. Physiol. Ren. Physiol.* 289, F1088–F1095. doi:10.1152/ajprenal.00474.2004
- Shimada, T., Kakitani, M., Yamazaki, Y., Hasegawa, H., Takeuchi, Y., Fujita, T., et al. (2004b). Targeted Ablation of Fgf23 Demonstrates an Essential Physiological Role of FGF23 in Phosphate and Vitamin D Metabolism. *J. Clin. Invest.* 113, 561–568. doi:10.1172/jci200419081
- Shimada, T., Urakawa, I., Yamazaki, Y., Hasegawa, H., Hino, R., Yoneya, T., et al. (2004a). FGF-23 Transgenic Mice Demonstrate Hypophosphatemic Rickets with Reduced Expression of Sodium Phosphate Cotransporter Type IIa. *Biochem. Biophys. Res. Commun.* 314, 409–414. doi:10.1016/j.bbrc.2003.12.102
- Silswal, N., Touchberry, C. D., Daniel, D. R., McCarthy, D. L., Zhang, S., Andresen, J., et al. (2014). FGF23 Directly Impairs Endothelium-dependent Vasorelaxation by Increasing Superoxide Levels and Reducing Nitric Oxide Bioavailability. *Am. J. Physiology-Endocrinology Metab.* 307, E426–E436. doi:10.1152/ajpendo.00264.2014
- Six, I., Okazaki, H., Gross, P., Cagnard, J., Boudot, C., Maizel, J., et al. (2014). Direct, Acute Effects of Klotho and FGF23 on Vascular Smooth Muscle and Endothelium. *PLoS One* 9, e93423. doi:10.1371/journal.pone.0093423
- Slavic, S., Ford, K., Modert, M., Becirovic, A., Handschuh, S., Baierl, A., et al. (2017). Genetic Ablation of Fgf23 or Klotho Does Not Modulate Experimental Heart Hypertrophy Induced by Pressure Overload. *Sci. Rep.* 7, 11298. doi:10.1038/s41598-017-10140-4
- Smith, E. R., Tan, S.-J., Holt, S. G., and Hewitson, T. D. (2017). FGF23 Is Synthesised Locally by Renal Tubules and Activates Injury-Primed Fibroblasts. *Sci. Rep.* 7, 3345. doi:10.1038/s41598-017-02709-w
- Urakawa, I., Yamazaki, Y., Shimada, T., Iijima, K., Hasegawa, H., Okawa, K., et al. (2006). Klotho Converts Canonical FGF Receptor into a Specific Receptor for FGF23. *Nature* 444, 770–774. doi:10.1038/nature05315
- Van Berlo, J. H., Maillet, M., and Molkenin, J. D. (2013). Signaling Effectors Underlying Pathologic Growth and Remodeling of the Heart. *J. Clin. Invest.* 123, 37–45. doi:10.1172/jci62839
- Van Venrooij, N. A., Pereira, R. C., Tintut, Y., Fishbein, M. C., Tumber, N., Demer, L. L., et al. (2014). FGF23 Protein Expression in Coronary Arteries Is Associated with Impaired Kidney Function. *Nephrol. Dial. Transpl.* 29, 1525–1532. doi:10.1093/ndt/gft523
- Verkaik, M., Juni, R. P., van Loon, E. P. M., van Poelgeest, E. M., Kweskeboom, R. F. J., Gam, Z., et al. (2018). FGF23 Impairs Peripheral Microvascular Function in Renal Failure. *Am. J. Physiology-Heart Circulatory Physiol.* 315, H1414–H1424. doi:10.1152/ajpheart.00272.2018
- Weber, T. J., Liu, S., Indridason, O. S., and Quarles, L. D. (2003). Serum FGF23 Levels in Normal and Disordered Phosphorus Homeostasis. *J. Bone Miner. Res.* 18, 1227–1234. doi:10.1359/jbmr.2003.18.7.1227
- Yilmaz, M. I., Sonmez, A., Saglam, M., Yaman, H., Kilic, S., Demirkaya, E., et al. (2010). FGF-23 and Vascular Dysfunction in Patients with Stage 3 and 4 Chronic Kidney Disease. *Kidney Int.* 78, 679–685. doi:10.1038/ki.2010.194
- Zacchigna, S., Paldino, A., Falcão-Pires, I., Daskalopoulos, E. P., Dal Ferro, M., Vodret, S., et al. (2021). Towards Standardization of Echocardiography for the Evaluation of Left Ventricular Function in Adult Rodents: a Position Paper of the ESC Working Group on Myocardial Function. *Cardiovasc. Res.* 117, 43–59. doi:10.1093/cvr/cvaa110
- Zhang, Y., Li, H., Wei, R., Ma, J., Zhao, Y., Lian, Z., et al. (2015). Endothelial Cells Regulate Cardiac Myocyte Reorganization through β 1-integrin Signaling. *Cell Physiol Biochem* 35, 1808–1820. doi:10.1159/000373992

Conflict of Interest: TT filed and licensed patents in the field of noncoding RNAs. TT is founder and shareholder of Cardior Pharmaceuticals GmbH.

The remaining authors declare that the research was conducted in the absence of any commercial or financial relationships that could be construed as a potential conflict of interest.

Publisher's Note: All claims expressed in this article are solely those of the authors and do not necessarily represent those of their affiliated organizations, or those of the publisher, the editors, and the reviewers. Any product that may be evaluated in

this article, or claim that may be made by its manufacturer, is not guaranteed or endorsed by the publisher.

Copyright © 2022 Eitner, Richter, Schwänen, Szaroszyk, Vogt, Grund, Thum, Heineke, Haffner and Leifheit-Nestler. This is an open-access article distributed under the terms of the Creative Commons Attribution License (CC BY). The use, distribution or reproduction in other forums is permitted, provided the original author(s) and the copyright owner(s) are credited and that the original publication in this journal is cited, in accordance with accepted academic practice. No use, distribution or reproduction is permitted which does not comply with these terms.